Journal of Computational and Applied Mathematics 466 (2025) 116595

Contents lists available at ScienceDirect

Journal of Computational and Applied Mathematics

journal homepage: www.elsevier.com/locate/cam

A compact scheme for the Munk boundary-layer equation in one dimension☆

M. Ben-Artzi [a], J.-P. Croisille [b,*], D. Fishelov [c]

[a] Institute of Mathematics, The Hebrew University, Jerusalem 91904, Israel
[b] Université de Lorraine, CNRS, IECL, Metz, F-57000, France
[c] Afeka College of Engineering, 218 Bnei-Efraim St., Tel Aviv 69107, Israel

ARTICLE INFO

MSC:
primary 65L10
secondary 65L70
34K28

Keywords:
Munk equation
Boundary layer
Compact scheme
Shishkin grid

ABSTRACT

In this paper, we introduce a two-scale compact finite difference scheme for the equation

$$\begin{cases} -\beta\dfrac{d}{dx}u+\varepsilon\left(\dfrac{d}{dx}\right)^4 u=f, \quad x\in(a,b) \\ u(a)=u(b)=u'(a)=u'(b)=0. \end{cases} \tag{MK-1D}$$

This equation serves as a model for the nonlinear barotropic equation (NB) governing oceanic flows.

$$\partial_t\Delta\psi+\nabla^\perp\psi.\nabla\Delta\psi+\beta\partial_x\psi=\frac{1}{H}(\nabla\times\tau)_v-\mu\Delta\psi+\varepsilon\Delta^2\psi, \tag{NB}$$

where $\psi(x,y,t)$ and τ are the streamfunction and the wind stress tensor, respectively. This equation encodes the *western boundary layer problem* (Ghil et al. 2008) for the potential vorticity ψ, which corresponds to the sharp contrast between the gyres flow in the oceanic circulation at mid-latitude and the strong western boundary currents. Numerical results for Equation (MK-1D) show that, with this two-scale scheme, high order accuracy is preserved for u and $\left(\frac{d}{dx}\right)u$ both in the boundary layer and in the central zone of the domain. The test cases are taken from Chekroun et al. 2020.

1. Introduction

The time dependent nonlinear barotropic dynamics equation is expressed as [1, Chap.3], [2]

$$\partial_t\Delta\psi+\nabla^\perp\psi.\nabla\Delta\psi+\beta\partial_x\psi=\frac{1}{H}(\nabla\times\tau)_v-\mu\Delta\psi+\varepsilon\Delta^2\psi. \tag{1.1}$$

The notation is as follows.

- $\psi(x,y,t)$ is the streamfunction and $\Delta\psi(t,x,y)$ is the vertical vorticity (Δ = 2D-Laplacian).
- $\nabla^\perp\psi=(-\partial_y\psi,\partial_x\psi)=(u,v)$ is the horizontal velocity. The convective term is $\nabla^\perp\psi.\nabla\Delta\psi=u\partial_x\Delta\psi+v\partial_y\Delta\psi$.
- $\varepsilon>0$ is the lateral eddy viscosity. It encodes the shear wind friction effect at the surface of the ocean.
- $\mu\geq 0$ is a viscosity modelling the friction at ocean bottom.

☆ The authors thank the Erwin Schrödinger International Institute for Mathematics and Physics for its support during the Thematic Program *The Dynamics of Planetary-Scale Flows* (Apr.11-Jun.02, 2023) and the organizers Profs. A. Constantin, D. Dritschel and N. Paldor.

* Corresponding author.
E-mail addresses: mbartzi@math.huji.ac.il (M. Ben-Artzi), jean-pierre.croisille@univ-lorraine.fr (J.-P. Croisille), daliaf@afeka.ac.il (D. Fishelov).

https://doi.org/10.1016/j.cam.2025.116595
Received 28 September 2024; Received in revised form 24 January 2025
Available online 27 February 2025

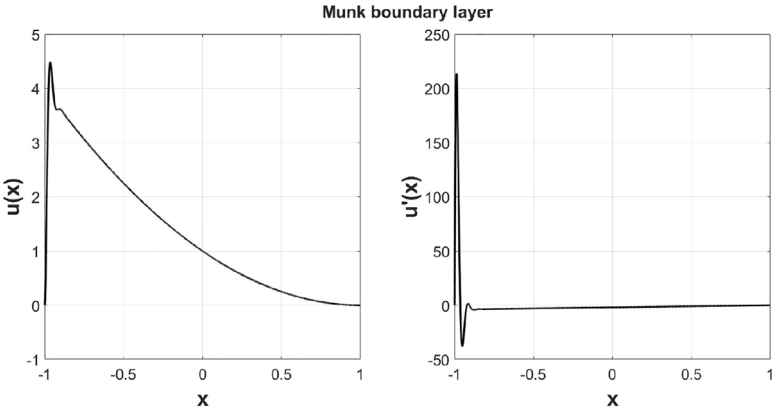

Fig. 1. A typical profile of a solution $u(x)$ (left panel) and $\frac{d}{dx}u(x)$ (right panel) of a Munk boundary layer. The function $u(x)$ is (2.9) with parameter $p = 2$. The boundary conditions are $u(-1) = u(1) = u'(-1) = u'(1) = 0$.

- $\beta > 0$ is the constant of the Coriolis force. It depends on the latitude at which the so-called beta-plane hypothesis is applied.
- H is the depth of the ocean, assumed here to be constant.
- τ is the surface wind stress.

Eq. (1.1) is a variant of the 2D Navier–Stokes equation in pure streamfunction formulation [3,4]. Assuming time independence, and that the convective term and bottom friction are negligible, leads to the two-dimensional linear problem posed e.g. in the rectangle $\Omega = (a, b) \times (c, d)$,

$$\begin{cases} -\beta\partial_x\psi(x,y) + \varepsilon\Delta^2\psi(x,y) = f(x,y), \quad (x,y) \in \Omega \\ \psi = \partial_n\psi = 0, \quad (x,y) \in \partial\Omega. \end{cases} \tag{MK-2D}$$

Assuming independence in y, one obtains the one-dimensional version of the problem: find $x \in (a, b) \mapsto u(x)$, solution of

$$\begin{cases} -\beta\dfrac{d}{dx}u + \varepsilon\Big(\dfrac{d}{dx}\Big)^4 u = f, \quad a < x < b, \quad (i) \\ u(a) = u(b) = u'(a) = u'(b) = 0, \quad (ii) \end{cases} \tag{MK-1D}$$

This is a biharmonic convection–diffusion problem, called the *Munk* equation with Dirichlet boundary conditions. The length parameter

$$\gamma = (\varepsilon/\beta)^{1/3} \tag{1.2}$$

relates the Coriolis force strength to the eddy diffusion. The problem considered here is the design of a highly accurate compact finite difference scheme, in order to approximate the two functions $u(x)$ and $\frac{d}{dx}u(x)$ depicted in Fig. 1 by solving (MK-1D) numerically. The scheme is designed to handle the limit $\gamma \to 0$. The smaller γ the thinner the boundary layer.

Concerning the scheme design, convergence analysis and test cases, our main reference is [5], where a detailed account is given on (MK-1D)–(MK-2D). Both the theoretical and numerical are treated therein, in the context of an "enriched" spectral scheme. See also [6] where a numerical analysis study of singular 4th order problems is presented. Refer also to the references therein. The Munk problem (MK-1D)–(MK-2D) is in general not covered in standard references on boundary layer analysis, where a second order viscous term is considered. In that case, the profile of the solution is monotonic, in contrast to Fig. 1. It has been the topic of many studies in mathematics, numerical analysis, and physics. Refer to the monographs [7] (mathematical analysis) and [8,9] (numerical analysis). There is of course an abundant literature in physics and oceanography related to the Munk model. In [10] a discussion of the Munk model regarding boundary conditions and numerical approximation is given. Another study [11], along with historical notes, presents the 2D Munk model in a rectangle, taking into account the aspect ratio. Finally, we refer to the nice editorial summary [12] for a recent account on boundary layer modelling in geophysical flows.

The outline of the paper is as follows. In Section 2, we present our reference scheme. Numerical results demonstrate that the error for u and u' are, as expected, fourth order. However, as observed in [5], a prohibitive grid size is required to be "layer-resolving". Section 3 addresses this issue in the framework of compact schemes. A two-scale compact scheme is proposed on a Shishkin grid with two stepsizes. The coarse stepsize fits the "offshore" zone (the gyre zone, called the CZ zone hereafter). The fine stepzise fits the thin boundary layer zone (called the BL zone). In Section 4 several numerical results, using the test series that were picked in [5], show that high accuracy is retained both in the BL and CZ zones. Section 5 draws some perspectives.

2. A compact scheme for the Munk equation

2.1. Design of the basic compact scheme

Consider the Munk equation

$$\Big(\mathcal{L}u(x) \triangleq\Big) - \beta \frac{d}{dx}u(x) + \varepsilon\Big(\frac{d}{dx}\Big)^4 u(x) = f(x), \quad x \in \mathbf{R}. \tag{2.1}$$

Denote $x_j = jh, j \in \mathbf{Z}$. A natural compact finite difference approximation for (2.1) is obtained as follows

(1) The derivative $\frac{d}{dx}u$ is approximated by the standard compact scheme

$$\sigma_x \tilde{\delta}_x u_j = \delta_x u_j. \tag{2.2}$$

The operators σ_x and δ_x are defined by

$$\sigma_x \phi_j \triangleq \frac{1}{6}\phi_{j-1} + \frac{2}{3}\phi_j + \frac{1}{6}\phi_{j+1}, \quad \delta_x \phi_j \triangleq (\phi_{j+1} - \phi_{j-1})/(2h). \tag{2.3}$$

(2) The fourth order derivative $(\frac{d}{dx})^4 u$ is approximated by the Discrete Biharmonic Operator (DBO) δ_x^4 [3,13,14]

$$\delta_x^4 u_j = \frac{12}{h^2}(\delta_x \tilde{\delta}_x u_j - \delta_x^2 u_j), \tag{2.4}$$

where $\delta_x^2 \phi_j = (\phi_{j+1} + \phi_{j-1} - 2\phi_j)/2h^2$. See also [15].

Using (2.2) and (2.4) yields the following approximation of (2.1) at node $j \in \mathbf{Z}$

$$\Big(\mathcal{L}_h u_j \triangleq\Big) - \beta\tilde{\delta}_x u_j + \varepsilon\delta_x^4 u_j = f_j, \quad j \in \mathbf{Z} \tag{2.5}$$

Since each operator $\tilde{\delta}_x$ and δ_x^4 has a 4th order truncation error, one expects a 4th order truncation error $\tau(u) = \Big(\mathcal{L}u\Big)^* - \mathcal{L}_h u^*$. One has[1]

$$\tau(u) = h^4\Big[\frac{\beta}{180}\Big((\frac{d}{dx})^5 u\Big)^* + \frac{\varepsilon}{720}\Big((\frac{d}{dx})^8 u\Big)^*\Big] + O(h^6). \tag{2.6}$$

Consider now the problem (MK-1D) on the bounded interval $I = (-1, 1)$. We use $N + 1$ nodes with stepsize $h = 2/N$, and the regular grid $x_j = -1 + jh$, $j \in [\![0, N]\!]$. Our reference scheme consists of applying (2.5) at interior nodes $j = 1, \dots, N-1$. A natural discrete counterpart of the 4 boundary conditions (MK-1D)(ii) is

$$u_0 = u_N = \tilde{\delta}_x u_0 = \tilde{\delta}_x u_N = 0. \tag{2.7}$$

With (2.7), there is no need of any ghost node or special treatment at the boundary. The final scheme is: solve for $[u_j], j \in [\![0, N]\!]$ the system

$$\begin{cases} -\beta\tilde{\delta}_x u_j + \varepsilon\delta_x^4 u_j = f_j, \quad j = 1, \dots, N-1, \\ \sigma_x \tilde{\delta}_x u_j = \delta_x u_j \quad j = 1, \dots, N-1, \\ u_0 = u_N = \tilde{\delta}_x u_0 = \tilde{\delta}_x u_N = 0. \end{cases} \tag{2.8}$$

This scheme is the natural extension to (MK-1D) of the DBO scheme [3, chap. 10.3]. Fourth order error estimate is expected [16]. Here however, we are interested in the specific regime $\beta \to \infty$ with $\varepsilon \to 0$, and such that $\gamma \to 0$. Oscillations are expected in the BL zone, and indeed they do appear. This problem is observed in Section 2.2.

2.2. Single grid numerical results

2.2.1. The CHT test case for the Munk equation

We consider the set of solutions (called CHT functions) (2.9) suggested in [5], defined by

$$u(x) = \Big(1 - \frac{1}{\sqrt{3}}Q_1(x,\gamma) - Q_2(x,\gamma)\Big)(1-x)^2, \quad x \in (-1, 1), \tag{2.9}$$

with

$$\begin{cases} Q_1(x,\gamma) = \exp\Big(-\frac{x+1}{2\gamma}\Big)\sin\Big(-\frac{\sqrt{3}(x+1)}{2\gamma}\Big), \\ Q_2(x,\gamma) = \exp\Big(-\frac{x+1}{2\gamma}\Big)\cos\Big(-\frac{\sqrt{3}(x+1)}{2\gamma}\Big). \end{cases} \tag{2.10}$$

[1] For u a given function, u^* denotes the gridfunction deduced from u by restriction to the grid.

Table 1
Test case (2.9) with $p = 1$ for the Munk equation (MK-1D). Relative maximum errors $|\mathfrak{e}|_\infty$ and $|\mathfrak{e}_x|_\infty$ are reported, when using (2.8). A standard 4th order accuracy is observed with good error levels.

mesh	20	Rate	40	Rate	80	Rate	160
$\|\mathfrak{e}\|_\infty$	4.3529(−3)	3.85	3.0202(−4)	3.99	1.9060(−5)	4.00	1.1940(−6)
$\|\mathfrak{e}_x\|_\infty$	7.4202(−3)	4.23	3.9564(−4)	4.06	2.3706(−5)	4.02	1.4659(−6)

The velocity β, viscosity ε and length γ are given by the sequence

$$(\beta_p, \varepsilon_p, \gamma_p) = (10^{2p}, 10^{-p}, 10^{-p}), \quad p \geq 0. \tag{2.11}$$

The function (2.9) provides a set of test cases with parameter p. The larger p, the smaller γ, the thinner the boundary layer and the more difficult the test problem. The forcing function f in (MK-1D) is obtained by (hand manufacturing method)

$$f(x) \triangleq \mathcal{L}u(x). \tag{2.12}$$

Refer to [5] for the expression of $f(x)$. Select first $p = 1$ in (2.11). This corresponds to $(\beta, \varepsilon, \gamma) = (100, 0.1, 0.1)$. In this case, Eq. (MK-1D) is a regular 4th order ODE. Table 1 exhibits an expected 4th order convergence rate as well as accurate error levels for u and $\frac{d}{dx}u$ using the coarse grid sequence $N = 20, 40, 80, 160$. The notation for the relative errors $\mathfrak{e}, \mathfrak{e}_x$ and for the maximum grid norm is

$$\begin{cases} \mathfrak{e}_j = |u^*(x_j) - \mathfrak{u}_j| / \max\limits_{-1<x<1} |u(x)|, \quad \mathfrak{e}_{x,j} = \left| \left(\dfrac{d}{dx} u \right)^* (x_j) - \tilde{\delta}_x \mathfrak{u}_j \right| / \max\limits_{-1<x<1} |u'(x)|, \\ |\mathfrak{v}|_\infty = \max\limits_{1 \leq j \leq N-1} |\mathfrak{v}_j|. \end{cases} \tag{2.13}$$

The cases $p = 2$ and $p = 3$ serve to illustrate the numerical difficulty with the scheme (2.8) for the Munk problem (MK-1D).

2.2.2. Case $p = 2$

This case corresponds to $(\beta, \varepsilon, \gamma) = (10^4, 10^{-2}, 10^{-2})$. Consider first the grid sequence $N = 20, 40, 80, 160$. This sequence is too coarse to approximate the BL zone, even qualitatively. Fig. 2 top shows the relative errors for u and $\frac{d}{dx}u$. Typical numerical oscillations are displayed with two subsequences observed. Note however that even with only two nodes in the boundary layer, the numerical derivative $\tilde{\delta}_x u$ displays a somehow acceptable behaviour, considering the magnitude of the function. With a grid size $N = 160$ (Fig. 2 bottom) the profiles of u and $\frac{d}{dx}u$ are accurately reproduced, with only 6 nodes in the BL zone. Fig. 3 exhibits convergence slopes for the unresolved grid sequence $N = 20, 40, 80, 160$ (top) and for the resolved grid sequence $N = 160, 320, 640, 1280$ (bottom). An expected order 4 for u and $\frac{d}{dx}u$ is observed. The two top panels show that some grid convergence slope in the max norm can be observed, even in the presence of an oscillating numerical solution.

2.2.3. Case $p = 3$

This case corresponds to $(\beta, \varepsilon, \gamma) = (10^6, 10^{-3}, 10^{-3})$. With $N = 400$, the scheme is layer-unresolved and oscillations similar to Fig. 3 top do appear, (not shown). The grid $N = 800$ displays a resolved BL zone. Fig. 4 top shows the convergence slopes for the unresolved grid sequence $N = 100, 200, 400, 800$. Fig. 3 bottom shows the case of the layer-resolved grid sequence $N = 800, 1600, 3200, 6400$.

2.3. Comments

Here are some observations drawn from the numerical results in Section 2.2.

(1) It is well known that discretizing $\mathcal{L} \triangleq \beta\partial_x - \varepsilon\partial_x^2$ by the centred operator $\mathcal{L}_h \triangleq \beta\delta_x - \varepsilon\delta_x^2$, leads to oscillations in the numerical boundary layer, see e.g. [17, Chap.3]. Here oscillations do appear when the value h/γ (the Peclet number in the present context) is large.
(2) For fixed values of ε and β a 4th order asymptotic convergence rate takes place when $h \to 0$. This is of little help in practice. In the case $p = 3$ a typical layer-resolved grid must be of size $N \simeq 4000$, as observed in Fig. 4. However, a grid of $N = 4000$ results in a matrix corresponding to (2.8), of size 8000×8000 (two unknowns per node), which is prohibitive for a 1D problem.
(3) A convergent slope in the maximum norm, possibly high order, is no guaranty that the results are accurate with the finest grid. An oscillating behaviour may still occur.

3. A two-scale compact scheme for the Munk equation

3.1. Two-domain compact scheme approach

We present an extension of the compact scheme (2.8) based on the splitting of the interval $I = (-1, 1)$ into two parts, see Fig. 5. Two contiguous grids are used, denoted as

$$\begin{cases} x_0^{\mathrm{BL}} \triangleq -1, x_1^{\mathrm{BL}} \triangleq -1 + h, \ldots, x_{N-1}^{\mathrm{BL}} \triangleq c - h, x_N^{\mathrm{BL}} \triangleq c \\ \bar{x}_0^{\mathrm{CZ}} \triangleq c, \bar{x}_1^{\mathrm{CZ}} \triangleq c + \bar{h}, \ldots, x_{\bar{N}-1}^{\mathrm{CZ}} \triangleq 1 - \bar{h}, x_{\bar{N}}^{\mathrm{CZ}} \triangleq 1. \end{cases} \tag{3.1}$$

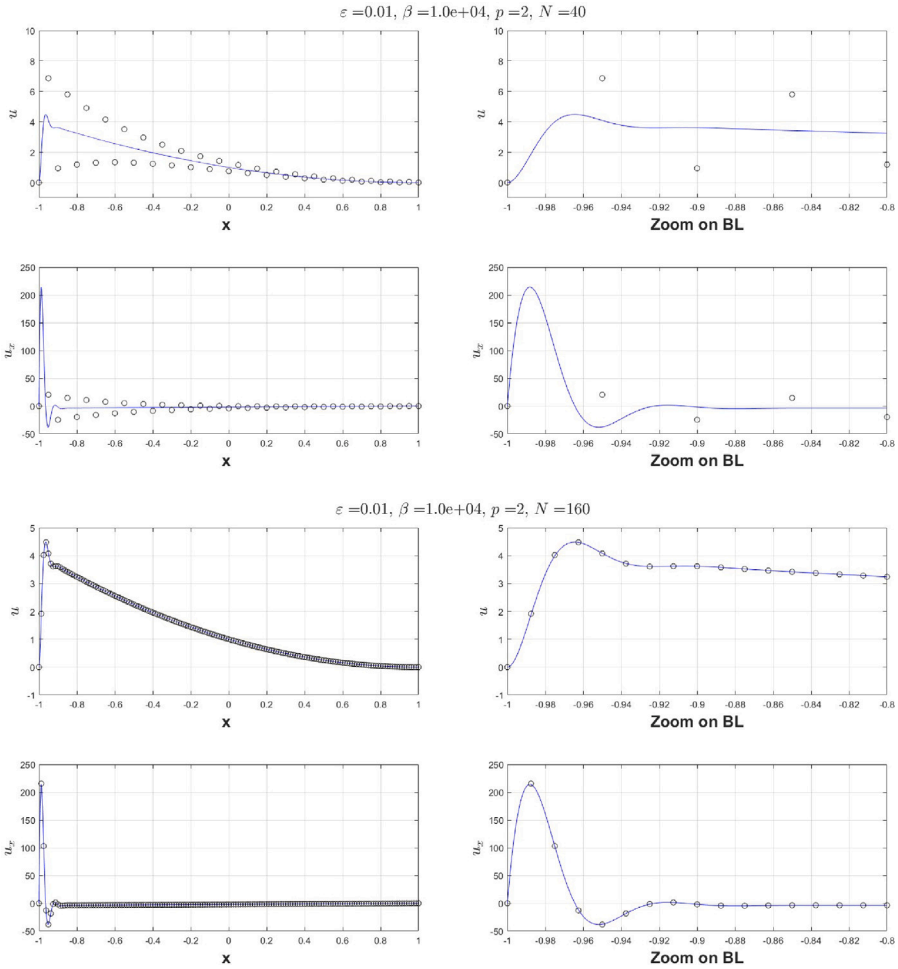

Fig. 2. Test case (2.9) with $p = 2$ for the Munk Eq. (MK-1D). Top: behaviour of the scheme for u and $\frac{d}{dx}u$ with the underresolved grid $N = 40$: the underresolution is characterized by two subsequences for the approximations of u and $\frac{d}{dx}u$. Bottom: behaviour of the scheme for u and $\frac{d}{dx}u$ with the grid $N = 160$. The results are satisfactory.

The interconnecting node $x_N^{\mathrm{BL}} = x_0^{\mathrm{CZ}} = c$ is called the *transmission* node. The basic scheme (2.8) is used in zones BL and CZ with stepsize h and $\bar{h}$, respectively. In what follows, we define a specific scheme at the transmission node c. This kind of two-scale grid belongs to the Shishkin grids category, (piecewise constant stepsize). See [8] and the references therein. Hereafter, we explore a scheme design based on a particular set of high order polynomials. Our guideline consists of the observed numerical errors obtained for (2.9) with low values of γ. In Section 3.2 we present the transmission scheme giving the most accurate results so far.

3.2. A two-scale extension of the discrete biharmonic operator

In Sections 3.2.1 and 3.2.2 interpolatory polynomials called $q(x)$ and $r(x)$ are introduced. They serve to define the operators $\widehat{\delta}_x$ and $\widehat{\delta}_x^4$, respectively, in the spirit of compact schemes. These operators are used at the transmission node c in (3.16) hereafter.

3.2.1. The polynomial $q \in \mathcal{P}_4$

Here and in Section 3.2.2, we call x_j a general grid with non equispaced stepsize. At each node is attached a couple of values $(u_j, u_{x,j})$ approximating $u(x_j)$ and $\frac{d}{dx}u(x_j)$, where u is a given function. Define as in [18] the polynomial $q \in \mathcal{P}_4$

$$q(x) = b_0 + b_1(x - x_j) + b_2(x - x_j)^2 + b_3(x - x_j)^3 + b_4(x - x_j)^4, \tag{3.2}$$

fitting the 5 data near x_j

$$\begin{cases} q(x_{j-1}) = u_{j-1}, \quad q(x_j) = u_j, \quad q(x_{j+1}) = u_{j+1}, \\ q'(x_{j-1}) = u_{x,j-1}, \quad q'(x_{j+1}) = u_{x,j+1}. \end{cases} \tag{3.3}$$

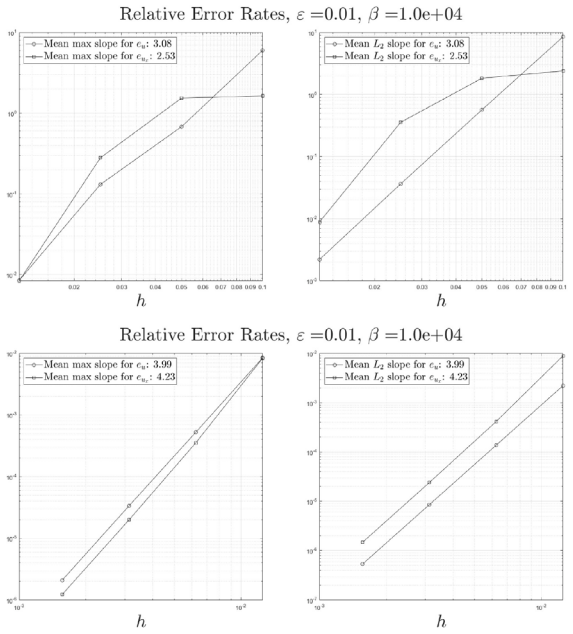

Fig. 3. Test case (2.9) with $p = 2$ for the Munk Eq. (MK-1D). Top panel: convergence rate for e and e_x with the grid sequence $N = 20, 40, 80, 160$. This grid sequence corresponds to an under-resolved BL. However, we can see that with a fine enough grid the numerical solution converges to the exact solution. Bottom panel: convergence rate for e and e_x with the grid sequence $N = 160, 320, 640, 1280$. This grid sequence corresponds to a resolved boundary layer. 4th order convergence for e and e_x is observed as well as error levels less than 10^{-6} for u and $\frac{d}{dx}u$.

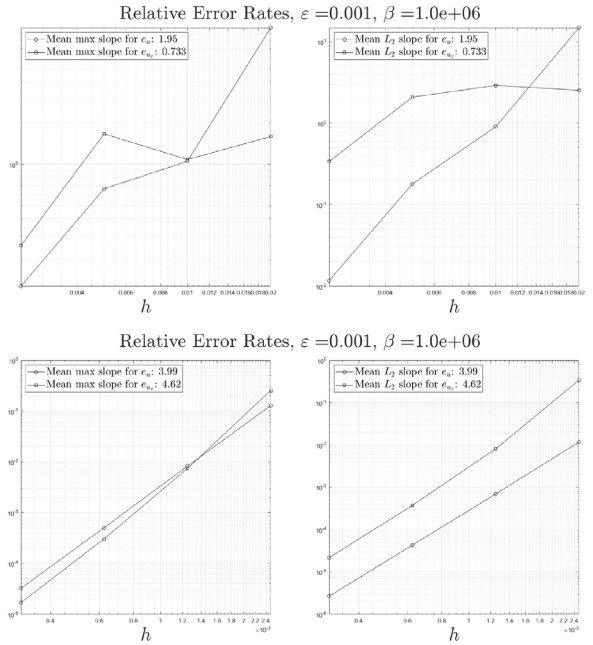

Fig. 4. Test case (2.9) with $p = 3$ for the Munk Eq. (MK-1D). Top panel: convergence rate for e and e_x with the grid sequence $N = 100, 200, 400, 800$. Underresolution can coexist with some convergence. Bottom panel: convergence rate for e and e_x with the grid sequence $N = 800, 1600, 3200, 6400$. This grid sequence corresponds to a resolved boundary layer. A 4th order convergence for e and e_x is observed.

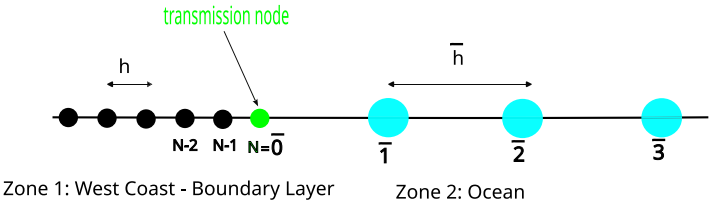

Fig. 5. Shishkin two-scale Finite Difference grid. Fine grid: $0 \le j \le N$; Coarse grid: $0 \le \bar{j} \le \bar{N}$. The transmission node is at $x_N = x_{\bar{0}} = c$.

With the definition $h_1 \triangleq x_j - x_{j-1}$ and $h_2 \triangleq x_{j+1} - x_j$ and

$$\begin{cases} \alpha_{1,j} = \dfrac{h_2^2}{(h_2+h_1)^2}, \quad \alpha_{2,j} = \dfrac{h_1^2}{(h_2+h_1)^2}, \quad \beta_{2,j} = \dfrac{2(h_2-h_1)}{h_1 h_2}, \\ \beta_{1,j} = -\dfrac{2h_2^2(2h_1+h_2)}{h_1(h_1+h_2)^3}, \quad \beta_{3,j} = \dfrac{2h_1^2(2h_2+h_1)}{h_2(h_1+h_2)^3}. \end{cases} \tag{3.4}$$

We obtain that the coefficient $b_1 = q'(x_j)$ in (3.2) is expressed as

$$b_1 = \beta_{1,j} u_{j-1} + \beta_{2,j} u_j + \beta_{3,j} u_{j+1} - (\alpha_{1,j} u_{x,j-1} + \alpha_{2,j} u_{x,j+1}). \tag{3.5}$$

Defining $\widehat{\delta}_x u_j \triangleq b_1$ extends to the irregular case the standard formula (2.2). It was proved in [18] that it is 4th order accurate with respect to $\frac{d}{dx}u(x_j)$, assuming uniform lower and upper bounds on h_1/h_2.

3.2.2. *The polynomial $r \in \mathcal{P}_7$ for $\widehat{\delta}_x^4$*

Consider the transmission node c. This node is the connecting node between the fine grid on the left and the coarse grid on the right, see Fig. 5. The ratio between the coarse grid $\bar{h}$ and the fine grid h is called

$$R \triangleq \bar{h}/h. \tag{3.6}$$

We assume that $R > 1$ ($\bar{h} > h$). In Section 3.2.1, a discrete derivative at the transmission node $\widehat{\delta}_x u_j$ has been defined, based on the polynomial $q(x)$ in (3.2). Here, we define and extended version of the Discrete Biharmonic Operator (DBO) called $\widehat{\delta}_x^4$ approximating $(\frac{d}{dx})^4(x_j)$. It is based on data carried by the two scale grid in Fig. 5. On a regular grid, observe that the DBO operator δ_x^4 satisfies at any internal node i the identity [3, Sect. 10.4]

$$\sigma_x \delta_x^4 u_i = (\delta_x^2)^2 u_i \tag{3.7}$$

The identity (3.7) amounts to "eliminate" $\tilde{\delta}_x u_i$ in (2.4). Call j the index of the node c. We have

$$x_j \triangleq c = x_N^{\mathrm{BL}} = \bar{x}_{\bar{0}}^{\mathrm{CZ}}, \tag{3.8}$$

Consider the identity (3.7) at node $x_{j-1} = c - h$,

$$\sigma_x \delta_x^4 u_{j-1} = (\delta_x^2)^2 u_{j-1}. \tag{3.9}$$

It is expressed as

$$\delta_x^4 u_j = \frac{6}{h^4}(u_{j+1} - 4u_j + 6u_{j-1} - 4u_{j-2} + u_{j-3}) - \delta_x^4 u_{j-2} - 4\delta_x^4 u_{j-1}. \tag{3.10}$$

Next, the identity (3.10) is used to *define* $\delta_x^4 u_j$ at the transmission node $c = x_j$. In (3.10), the nodes with index $j-3, j-2, j-1$ are on the left of $c = x_j$ (the BL zone). They carry the values $u_{j-3}, u_{j-2}, u_{j-1}$, respectively. In the contrary $x_{j+1} = c + h$ is the only node on the right of c. It does not belong to the coarse grid (assuming $\bar{h} > h$), and does not carry any value. Therefore in (3.10) the value u_{j+1} is not known. It must be interpolated. This is done using a Lagrange polynomial $r(x) \in \mathcal{P}_7$

$$\begin{aligned} r(x) = {} & a_0 + a_1(x-c) + a_2(x-c)^2 + a_3(x-c)^3 + a_4(x-c)^4 \\ & + a_5(x-c)^5 + a_6(x-c)^6 + a_7(x-c)^7 \end{aligned} \tag{3.11}$$

Suppose data $f(x)$ is known at the 8 nodes $x \in \{c-4h, c-3h, c-2h, c-h, c, c+\bar{h}, c+2\bar{h}, c+3\bar{h}\}$. The 8 coefficients a_k, $k \in [\![0,7]\!]$ are obtained by the 8 equations

$$\begin{cases} r(c) = f(c), \quad r(c-h) = f(c-h), \quad r(c+\bar{h}) = f(c+\bar{h}), \\ r(c-2h) = f(c-2h), \quad r(c-3h) = f(c-3h), \quad r(c-4h) = f(c-4h), \\ r(c+2\bar{h}) = f(c+2\bar{h}), \quad r(c+3\bar{h}) = f(c+3\bar{h}). \end{cases} \tag{3.12}$$

Next, $f(c+h)$ is interpolated by

$$\tilde{u}_{j+1} \triangleq r(x_j + h). \tag{3.13}$$

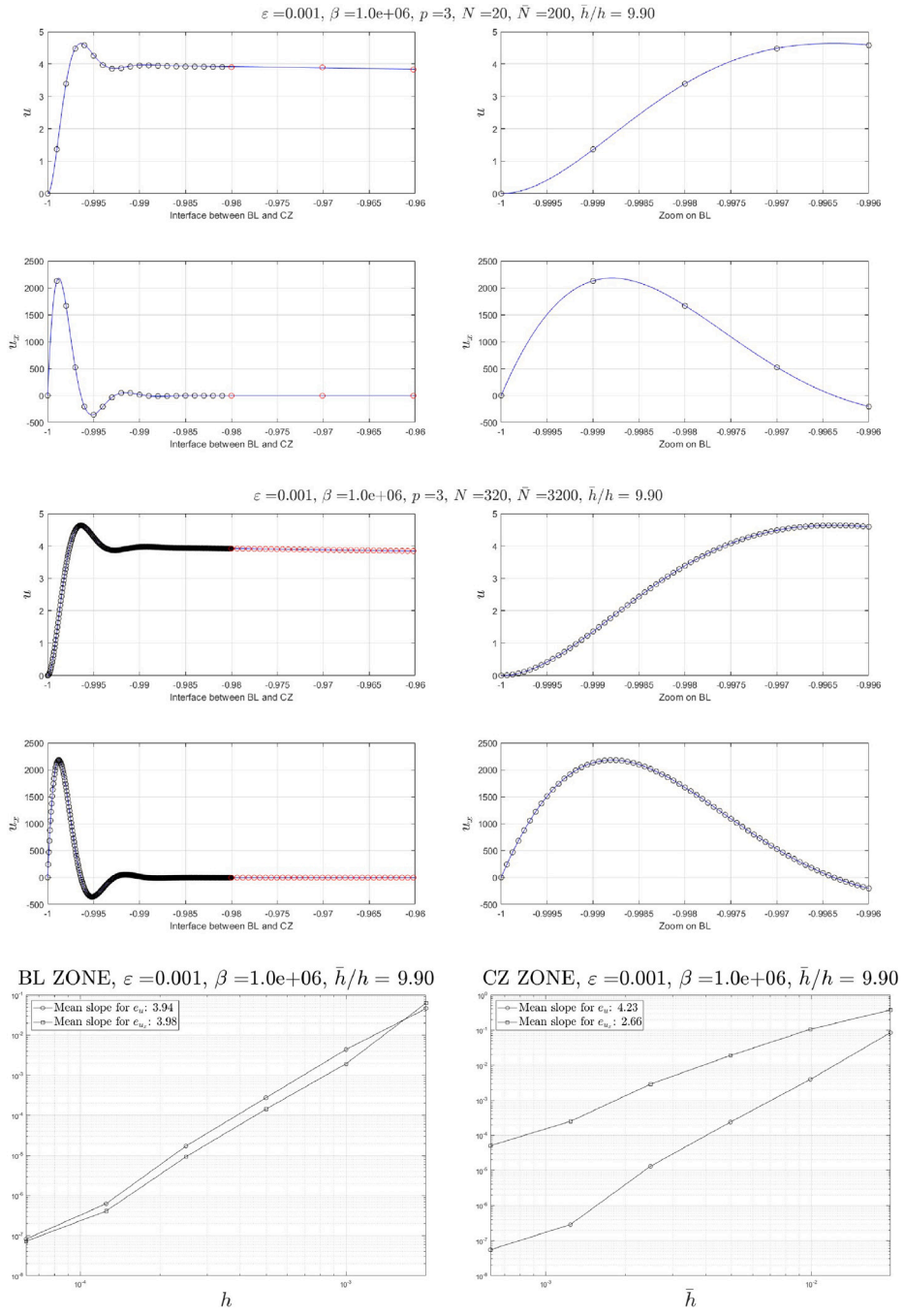

Fig. 6. Munk-Stommel Eq. (MK-1D) discretized with the scheme (3.16). Test case (2.9) with $p = 3$, $\varepsilon = 10^{-3}$, $\beta = 10^6$, $\gamma = 10^{-3}$. Coarse to fine grid ratio $\bar{h}/h = R = 10$. Convergence is analysed with grid sequence $(N, \bar{N})$ is $(10, 100), (20, 200), (40, 400), (80, 800), (160, 1600), (320, 3200)$. The transmission node is located at $c = -0.98$. The convergence rate is around 4 in BL and the CZ zones. The maximum relative error is close to 10^{-7} for u and u' in the BL and CZ zones with the finest grid.

Invoking $\tilde{u}_{j+1}$ defined in this way, the extended DBO is defined by (see (3.10)),

$$\widehat{\delta}_x^4 u_j \triangleq \frac{6}{h^4}(\tilde{u}_{j+1} - 4u_j + 6u_{j-1} - 4u_{j-2} + u_{j-3}) - \delta_x^4 u_{j-2} - 4\delta_x^4 u_{j-1}. \tag{3.14}$$

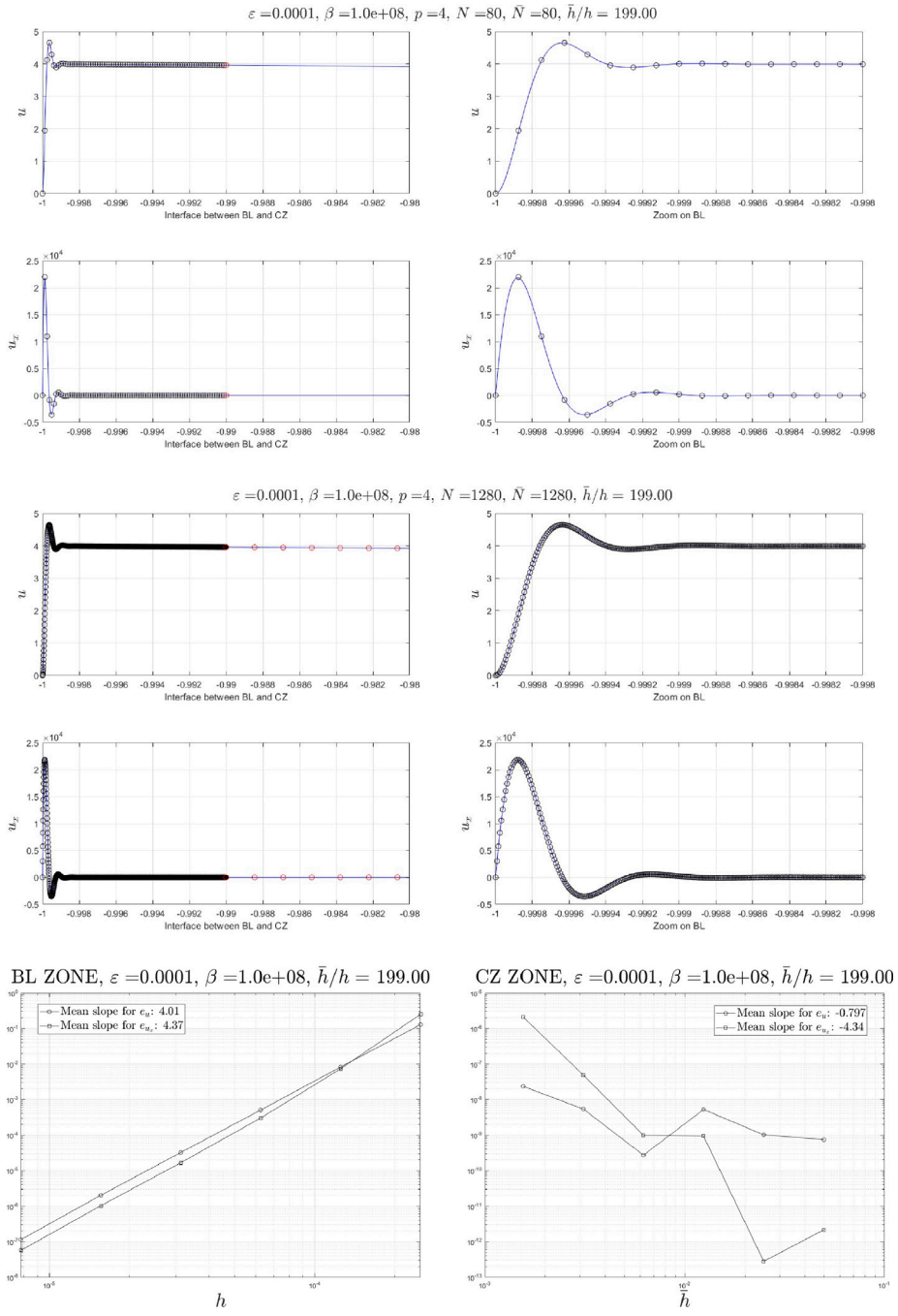

Fig. 7. Munk-Stommel Eq. (MK-1D) discretized with the scheme (3.16). Test case (2.9) with $p = 4$, $\varepsilon = 10^{-4}$, $\beta = 10^{8}$, $\gamma = 10^{-4}$. Coarse to fine grid ratio $\bar{h}/h = R \simeq 200$. Convergence is analysed with grid sequence $(N, \bar{N})$ is $(40, 40), (80, 80), (160, 160), (320, 320), (640, 640), (1280, 1280)$. The transmission node is located at $c = -0.99$. The convergence rate is around 4 in the BL zone for u and $\frac{d}{dx}u$. The computer accuracy is obtained in the CZ zone. The maximum relative error is close to 10^{-7} for u and u' in the BL zone.

Assume $h < \bar{h}$ with $R = \bar{h}/h > 1$. A 4-th order truncation, in the periodic setting, of the extended DBO is expressed in terms of h and R by

$$\widehat{\delta}_x^4 u_j - \left((\frac{d}{dx})^4 u\right)_j^* = \frac{1}{5040}(540R^3 - 990R^2 + 540R - 97)\left((\frac{d}{dx})^8 u\right)_j^* h^4 + O(h^5). \tag{3.15}$$

The truncation of the standard DBO (2.4) is recovered in the particular case $R = 1$.

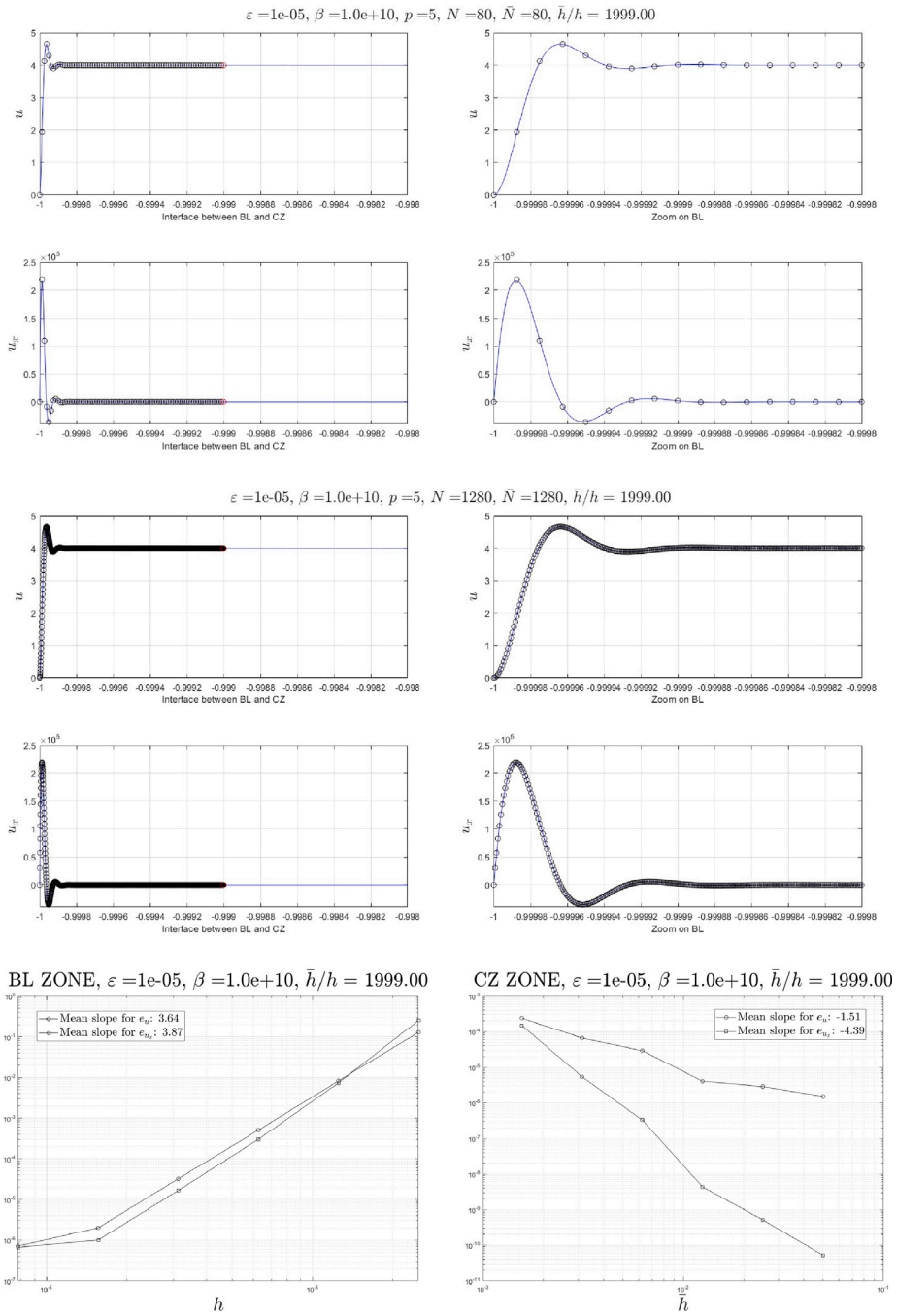

Fig. 8. Munk-Stommel Eq. (MK-1D) discretized with the scheme (3.16). Test case (2.9) with $p = 5$, $\epsilon = 10^{-5}$, $\beta = 10^{10}$, $\gamma = 10^{-5}$. Coarse to fine grid ratio $\bar{h}/h = R \simeq 2000$. Convergence is analysed with grid sequence $(N, \bar{N})$ is $(40, 40), (80, 80), (160, 160), (320, 320), (640, 640), (1280, 1280)$. The transmission node is located at $c = -0.999$. The convergence rate is around 4 in the BL zone. The computer accuracy is obtained in the CZ zone with coarse grids, but deteriorates with refinement (rounding errors). A maximum relative error close to 10^{-5} for u and u' in both zones can be reached.

3.3. Two-scale compact scheme for the Munk equation

Consider again Eq. (MK-1D). Let $c \in (-1, 1)$ be fixed. Recall that a fine grid with N intervals covers the BL zone $(-1, c)$ with stepsize $h = (c-(-1))/N$ and a coarse grid is layed out on $(c, 1)$ with $\bar{N}$ intervals and $\bar{h} = (1-c)/\bar{N}$. Assume $h < \bar{h}$ with $R = \bar{h}/h > 1$.

The full grid contains $N+\bar{N}$ intervals in all on $(-1,1)$. The Eq. (MK-1D) is approximated with the scheme

$$\begin{cases} -\beta\tilde{\delta}_x u_j + \varepsilon\delta_x^4 u_j = f_j^*, \quad 1 \le j \le N-1, \quad x_j \in (-1,c), \quad \text{BL zone} \\ -\beta\widehat{\delta}_x u_N + \varepsilon\widehat{\delta}_x^4 u_N = f_N^*, \quad x_N = c = \text{ transmission node} \\ -\beta\tilde{\delta}_x u_j + \varepsilon\delta_x^4 u_j = f_j^*, \quad N+1 \le j \le N+\bar{N}-1, \quad \text{CZ zone} \\ u_0 = u_{N+\bar{N}} = \widetilde{\delta}_x u_0 = \widetilde{\delta}_x u_{N+\bar{N}} = 0. \end{cases} \tag{3.16}$$

The scheme (3.16) is obtained by using (2.8) with the operators $\tilde{\delta}_x$ and δ_x^4 at the $N-1$ nodes in $x_j \in (a,c)$ with step size h. And similarly at the $\bar{N}-1$ nodes $x_j \in (c,1)$ with step-size $\bar{h}$. The hybrid scheme using the operators $\widehat{\delta}_x$ and $\widehat{\delta}_x^4$ is used only at the transmission node $x_N = c$. The linear system to be solved consists of the $N+\bar{N}-1$ Eqs. (3.16) and of the $N+\bar{N}-1$ equations relating the Hermitian derivative $\tilde{\delta}_x u_j$ to the values u_j. This is another $N+\bar{N}-1$ equations. Adding the 4 boundary conditions, yields a linear system of size $(2N+2\bar{N})\times(2N+2\bar{N})$.

4. Numerical results

In this section, we show numerical results for the scheme (3.16) to approximate (MK-1D) on the interval $(a,b)=(-1,1)$. The test (2.9) with the values $p=3,4,5$. For these three values, the single grid scheme (2.8) is not practical since the required number of nodes to obtain accuracy is prohibitive. In each case, the test has been performed with the following empirical principles.

1- The transmission node $c=x_N$ is located sufficiently far from the BL zone. A factor of at least 10 times the width of the BL zone has been found appropriate.
2- The computer accuracy has been reached as much as possible in the CZ zone. This has been found a good indicator that the results are accurate as well in the BL zone.

Figs. 6, 7 and 8 display results for $p=3$, $p=4$ and $p=5$, respectively. In each case and for each grid sequence, we have:

1- The shape in the transition zone as well as a zoom in the BL zone for $u(x)$ and $\frac{d}{dx}u$ is shown, for a coarse and a fine grid. The coarse to fine ratio $R=\bar{h}/h$ is given as well as the location of the transmission node c.
2- The convergence rates of the relative errors in the zones BL and CZ for u and $\frac{d}{dx}u$ for the maximum norm are shown. The l^2 norm has a similar shape and is not shown.
3- The values $p=4$ and $p=5$ correspond to a very sharp behaviour in the BL zone. This is the most difficult cases [5]. The coarsest grid almost solves the CZ zone at computer accuracy. It is observed that this induces 4th order convergence in the BL zone.

5. Conclusion

In this paper, a compact scheme for the Munk equation with a thin boundary layer has been introduced. Our goal is to investigate how to preserve the high accuracy of the compact DBO in a two-scale Cartesian grid setting. Numerical results obtained so far seem promising. Our scheme is an alternative to the "enriched" approach in [5], where an analytical knowledge of the layer is introduced in the approximation. In terms of finite differencing, our focus has been the investigation of strategies yielding better accuracy for the solution u and the derivative $\frac{d}{dx}u$. Regarding boundary layer approximations, the experimental point of view is considered important (see [8]), both for the scheme design and for the convergence analysis. Future work includes continuing our experimental analysis for (MK-1D), (MK-2D) and for nonlinear variants using multiscale grids. However, the numerical analysis seems a difficult question. In this regard, analytical tools in [8,9,19–22] will be obviously useful.

Data availability

Data will be made available on request.

References

[1] J. McWilliams, Oceanic circulation, 2006, AOS25 Courses Notes.
[2] M. Ghil, M.D. Chekroun, E. Simonnet, Climate dynamics and fluid mechanics: natural variability and related uncertainties, Phys. D 237 (2008) 2011–2126.
[3] M. Ben-Artzi, J.-P. Croisille, D. Fishelov, Navier–Stokes Equations in Planar Domains, Imp. Coll. Press, 2013.
[4] M. Ben-Artzi, J.-P. Croisille, D. Fishelov, A cartesian compact scheme for the Navier–Stokes equations in streamfunction formulation in irregular domains, J. Sci. Comp. 81 (3) (2019) 1386–1408.
[5] M.D. Chekroun, Y. Hong, R.M. Temam, Enriched numerical scheme for singularly perturbed quasi-geostrophic equations, J. Comput. Phys. 416 (2020) 109493.
[6] S. Franz, H.-G. Roos, Robust error estimation in energy and balanced norms for singularly perturbed fourth order problems, Comp. Math. Appl. 72 (2016) 233–247.
[7] G.-M. Gie, M. Hamouda, C.-Y. Jung, R.M. Temam, Singular Perturbations and Boundary Layers, in: AMS, vol. 200, Springer, 2018.
[8] P.A. Farrell, A.E. Hegarty, J.J.H. Miller, E. O'Riordan, G.I. Shishkin, Robust Computational Techniques for Boundary Layers, First Ed., Chapman and Hall CRC, 2000.
[9] H.-G. Roos, M. Stynes, L. Tobiska, Robust Numerical Methods for Singularly Perturbed Differential Equations, Springer-Verlag, Berlin, 2008.

[10] G. Badin, A.M. Barry, F. Cavallini, F. Crisciani, A new integration of Munk's linear model of wind-driven ocean circulation, Eur. Phys. J. Plus 127 (2012) 45.
[11] K. Gianchandani, H. Gildor, N. Paldor, On the role of domain aspect ratio in the westward intensification of wind-driven surface ocean circulation, Ocean. Sci. 17 (2021) 351–363.
[12] J. Kuehl, Editorial summary: Boundary layer processes in geophysical/environmental flows, Fluids 8 (2023) 279.
[13] M. Ben-Artzi, J.-P. Croisille, D. Fishelov, Convergence of a compact scheme for the pure streamfunction formulation of the unsteady Navier–Stokes system, SIAM J. Numers. Anal. 44 (5) (2006) 1997–2024.
[14] M. Ben-Artzi, G. Katriel, Spline functions, the biharmonic operator and approximate eigenvalues, Numer. Math. 141 (2019) 839–879.
[15] J.W. Stephenson, Single cell discretizations of order two and four for biharmonic problems, J. Comput. Phys. 55 (1984) 65–80.
[16] D. Fishelov, M. Ben-Artzi, J.-P. Croisille, Recent advances in the study of a fourth-order compact scheme for the one-dimensional biharmonic equation, J. Sci. Comp. 53 (2012) 55–79.
[17] C. Johnson, Numerical Solutions of Partial Differental Equations by the Finite Element Method, Cambridge Univ. Press, 1987.
[18] M. Ben-Artzi, I. Chorev, J.-P. Croisille, D. Fishelov, A compact difference scheme for the biharmonic equation in planar irregular domains, SIAM J. Numer. Anal. 47 (2009) 3087–3108.
[19] M. Ben-Artzi, J.-P. Croisille, D. Fishelov, R. Katzir, Discrete fourth-order Sturm–Liouville problems, IMA J. Numer. Anal. 38 (2018) 1485–1522, http://dx.doi.org/10.1093/imanum/drx038.
[20] M. Ben-Artzi, B. Kramer, Finite difference approach to fourth-order linear boundary value problems, IMA J. Numer. Anal. 41 (2021) 2530–2561, http://dx.doi.org/10.1093/imanum/draa057.
[21] D. Fishelov, J.-P. Croisille, Optimal convergence for time dependent Stokes equation: A new approach, J. Sci. Comp. 89 (2021) http://dx.doi.org/10.1007/s10915-021-01684-955--79.
[22] B.S. Jovanović, E. Suli, Analysis of Finite Difference Schemes for Linear Partial Differential Equations, Springer, 2014.